Int. J. Heat Mass Transfer. Vol. 35, No. 10, pp. 2605–2616, 1992
Printed in Great Britain

0017-9310/92 $5.00 + 0.00

Effects of condensation and liquid transport on the thermal performance of fibrous insulations

N. E. WIJEYSUNDERA and M. N. A. HAWLADER
Department of Mechanical & Production Engineering, National University of Singapore, 10 Kent Ridge Crescent, Singapore 0511

(*Received* 9 *October* 1990 *and in final form* 13 *September* 1991)

Abstract—The moisture gain by a fibrous insulation slab from a humid ambient is simulated under laboratory conditions. The liquid distribution, the total moisture gain, the heat flux and the temperature distribution are measured for a range of experimental conditions. The testing times ranged from 300 to 600 h. The physical processes involved in liquid transport are identified. Initially the total moisture gain increases nearly linearly with time and then decreases gradually. The heat flux shows a very gradual increase with time. The semi-empirical model used gives reasonable predictions of some of the measured quantities.

INTRODUCTION

FIBROUS materials are used widely as insulations and building sections in commercial and industrial applications. Fibreglass, in particular, is used in air conditioning systems to insulate chilled water pipes and cold air ducts. In these applications, vapour barriers are needed to prevent the migration of water vapour towards the cold surface from the ambient. The condensation of water vapour in the insulation usually results in the corrosion of the insulated duct and the eventual destruction of the insulation system. Other moisture related problems in buildings in hot humid climates are summarized by Lotz [1]. It is, therefore, important from a design stand-point to understand the effects of condensation and liquid transport on the thermal performance of insulations.

The effect of moisture on the thermal conductivity of insulations has been the subject of several investigations [2–4]. The main purpose of these studies was to establish satisfactory techniques for the measurement of the thermal conductivity of moisture laden insulations. Langlais *et al.* [5] pointed out the importance of considering the moisture redistribution process when the results of thermal conductivity measurements for such insulations are interpreted. Studies on vapour diffusion and condensation in fibreglass insulations were reported by several investigators [6–9]. In the foregoing studies, moisture was introduced into the insulation specimen by spraying water on it before the measurement was made.

Modi and Benner [10, 11] studied the effect of moisture gain on the thermal conductivity of spray-applied insulations. In this case, the moisture was absorbed from the humid ambient outside. Wijeysundera *et al.* [12, 13] measured the vapour flux and other important heat transfer parameters for an insulation slab under two sets of boundary conditions and operating schedules. Due to the relatively short duration of these experiments (about 60 h), there was no liquid transport in the insulation.

The movement of liquid within fibrous insulations has received less attention in the literature. The diffusion of liquid due to capillary pressure under isothermal conditions was investigated by Motakef and El-Masri [14], and Timusk and Tenende [15]. The foregoing studies showed the liquid movement in the direction of the fibres to be much larger than the movement perpendicular to the orientation of the fibres. Studies on the combined heat and vapour diffusion in fibrous insulations under different environmental conditions was reported by Crausse *et al.* [16].

Analytical studies on the condensation process in insulations were reported by Ogniewicz and Tien [17], and Motakef and El-Masri [18], who used one-dimensional quasi-steady models. Shapiro and Motakef [19] developed an unsteady model for moisture transfer in porous slabs. Vafai and Sarkar [20] used a detailed one-dimensional model in their numerical simulation. Detailed two-dimensional, transient, numerical simulations of condensation and moisture transfer in porous slabs were reported by Vafai and Whitaker [21], Vafai and Tien [22], and Tien and Vafai [23].

In the present study, the experimental work reported in refs. [12, 13] was extended to include the transport of the liquid phase. Insulation slabs absorbed moisture from an external humid ambient and the condensate produced at the cold plate was transported by the fluid pressure generated at the cold plate. Tests were carried out over a period of about 10–20 days. The distribution of the liquid phase, the heat flux, the temperature distribution and the total moisture gain were measured for several operating conditions. A semi-empirical model was used to interpret some of the experimental results.

In the next section of the paper the experimental apparatus and the procedure are described. The sub-

NOMENCLATURE

a	constant in Clausius–Clapeyron relationship (equation (2)) [K^{-1}]
c	mean specific heat capacity of slab [kJ kg^{-1} K^{-1}]
$C(z)$	concentration of water vapour [kg kg (dry air)$^{-1}$]
$\bar{C}$	constant in Clausius–Clapeyron relationship [kg kg^{-1}]
C_a	vapour concentration in chamber [kg kg (dry air)$^{-1}$]
$D_0(\theta)$	diffusion coefficient of vapour in slab [m^2 s^{-1}]
D_a	diffusivity of water vapour–air mixture [m^2 s^{-1}]
$D_L(\theta)$	diffusion coefficient of liquid in slab [m^2 s^{-1}]
$g(T)$	function of Clausius–Clapeyron relationship [kg kg^{-1}]
g'	$=dg/dT$ [kg kg^{-1} K^{-1}]
h	heat transfer coefficient between chamber air and insulation surface [W m^{-2} K^{-1}]
h_m	mass transfer coefficient between chamber air and insulation surface [kg m^{-2} s^{-1}]
h_{fg}	specific enthalpy of phase change [kJ kg^{-1}]
J	liquid water flux [kg m^{-2} s^{-1}]
$k(\theta)$	thermal conductivity of slab [W m^{-1} K^{-1}]
k_d	thermal conductivity of dry slab [W m^{-1} K^{-1}]
k_ω	thermal conductivity of water [W m^{-1} K^{-1}]
L	total thickness of slab [m]
L_d	thickness of dry region of slab [m]
q_L	heat flux at cold plate [W m^{-2}]
q_d	heat flux in dry region [W m^{-2}]
t	time [s]
$T(z)$	temperature of distribution slab [K]
T_a	temperature of air in chamber [K]
V	volume fraction of water (m^3 per m^3 of dry slab)
$X(\theta)$	function in equation (16) [W m^{-1} K $^{-1}$]
Y	function in equation (18)
z	distance along slab [m].

Greek symbols

Γ	condensation rate [kg m^{-3}]
ΔW	total moisture gain of slab [kg m^{-3}]
$\Delta\tau$	time between measurements [s]
$\varepsilon_v(\theta)$	void fraction of slab with liquid
ε_f	fibre volume fraction in dry slab
θ	mass liquid per unit volume of dry slab [kg m^{-3}]
θ_d	value of θ at wet–dry interface [kg m^{-3}]
ρ_a	local density of moist air [kg m^{-3}]
ρ_ω	density of water [kg m^{-3}]
ρ	mean local density of slab [kg m^{-3}]
τ	tortuosity factor
ϕ_d	vapour flux in dry region [kg m^{-2} s^{-1}].

sequent sections give the analysis and the results of the tests.

EXPERIMENTAL ARRANGEMENT AND PROCEDURE

Figure 1 shows a schematic diagram of the experimental arrangement. The warm humid ambient outside the insulation surface was provided by the well insulated air space above the exposed water surface of a constant temperature water bath. The bath was equipped with a controller which maintained the water temperature within ± 0.1°C of the set point value. This arrangement does not allow the independent control of the relative humidity in the air space. However, the relative humidity remained at a nearly constant level determined by the water temperature, over the entire duration of the tests.

The relative humidity was recorded using a Vaisala humidity sensor with an uncertainty of about $\pm 3\%$. The fluctuation of the relative humidity was about $\pm 3\%$.

The cold surface was provided by a heat sink which was essentially a fin-tube heat exchanger built within thick brass plates. The area of the heat sink surface was 450×450 mm and it was supplied with water from a constant temperature liquid bath, which maintained the liquid temperature within ± 0.1°C of the present value. The heat sink was attached to two beams which had holes that passed through four threaded rods. Nuts were provided for level adjustment.

The rods were fastened securely to a separate structure that moved on caster wheels. This arrangement facilitated the quick movement of the heat sink from above the test cavity to provide access to the insulation slab.

The design of the heat flow measuring 'pad' followed the recommendations provided in the ASTM guide lines for heat flow meter apparatus [24]. The heat flow meter, 100×100 mm and thickness 2 mm, was placed in a square cut-out in a rubber sheet of nominally the same thickness. The rubber acted as a side guard against lateral heat flow into the heat flow meter. Two thin rubber sheets were placed on either side of the heat flow meter to obtain good thermal contact between the bearing surfaces. Copper–

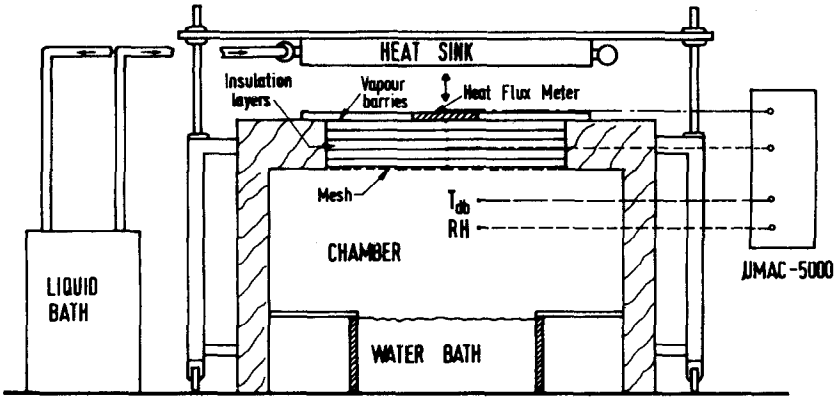

FIG. 1. Schematic diagram of the experimental set-up.

constantan thermocouples were installed on either surface of the heat flow measuring pad.

A typical insulation slab tested had a total thickness of about 80.0 mm before it was placed in the test cavity above the humid air chamber. The thickness of the slab was reduced to about 76.0 mm when the heat sink surface was in place. The slab was made up of five separate layers. Several tests were performed on a separate heat flow meter apparatus to determine the effect of assembling five layers on the thermal conductivity of the resultant slab. The commercially manufactured insulation layers used in the experiments had a surface unevenness of a few millimeters. When compressed by the heat sink surface the layers formed a continuous slab with negligible contact thermal resistance as evidenced by the linear temperature distribution obtained under steady state conditions.

A thin vapour barrier was spray-applied on the edges of each slab. A plastic barrier was applied to the top surface of the slab that was against the cold plate. This was to eliminate any water vapour flow from the sides and the top. The insulation slab had a cross-sectional area of 360×360 mm; but the area of the exposed bottom surface was only 330×330 mm. The outer rectangular area was left as an edge guard.

Copper–constantan thermocouples were placed at the mid-points of the interfaces between layers before they were assembled to form the slab. The slab was placed in the square cavity above the humid air space, and it was supported at the bottom by two taut nylon strings stretched diagonally across the square section of the cavity. This arrangement provided adequate support for the slab to prevent it from sagging when pressure was applied from top. The cavity was insulated on the outside with thick blocks of polystyrene. The heat flow from the edges is estimated to be less than about 1% of the measured heat flow.

The output voltages from the heat flux meter and the various thermocouples were recorded through appropriate interfaces in the μ-mac 5000 data acquisition and control system from Analog Devices Corporation. The data was processed in an IBM-PC-AT computer that was interfaced to the μ-mac system.

In the first series of calibration tests, the surface of the water bath was covered to prevent evaporation and the air space was used as the heat source. These tests were done with a standard insulation specimen from National Bureau of Standards of U.S.A. [25]. The thermal resistance values obtained from these tests were useful in establishing the accuracy of the calibration curve for the heat flux meter. The thermocouples were calibrated separately using a temperature calibration set-up.

At the beginning of a 'wet test', the insulation slab was weighed layer by layer. These were assembled and placed in the cavity with the thermocouples in the interfaces. The temperatures of the water baths were set at the desired values and the temperatures and the heat flux were recorded continuously.

At approximately 24 h intervals, the heat sink surface was lifted off the cavity by turning the nuts on the threaded rods. The structure was wheeled out to expose the insulation slab. The slab was carefully lifted out of the cavity and placed on a precision electronic balance. Fine threads were provided on the edges of each insulation layer to just lift it so that the total weight of the layers below it could be recorded. From these observations, the weight of each layer and thus the mass of liquid in each layer was determined. The slab was then placed quickly back in the cavity to continue the test. With experience, this procedure proved to be very convenient and effective in determining the liquid distribution in the insulation slab. The time required for the measurement was about 10 min, which was relatively short compared to the testing time of about 24 h.

In order to determine the effect of the disturbance caused during the measurement, some tests were repeated with weighing done only at the end of 190 and 310 h. The temperature and heat flux variations for the two tests agreed with those for continuous weighing, within the fluctuations of the measurement.

The corresponding liquid collection rate for the two cases agreed within about 4–5%. These tests showed that the disturbance caused during the 10 min measurement time had only a small effect on the measured quantities.

Two additional tests were done to trace the passage of water through the slab. In these tests, a water soluble dye, nigrosin, was applied to the inner side of the plastic vapour barrier at the cold plate. As liquid condensed at this surface, the dye diffused through the water to the various layers below. At the end of the run, the distribution of the dye gave a qualitative picture of the liquid distribution in the slab.

In the next section, a semi-empirical model to interpret some of the experimental data will be presented.

SEMI-EMPIRICAL MODEL

A comprehensive interpretation of the present experimental data will require two-dimensional numerical simulations of the form reported by Vafai and Tien [22]. This is not within the scope of the present study, which is mainly experimental. However, some qualitative comparisons will be made between the present results and those of Vafai and Tien [22]. The model used here for the interpretation of the experimental data is an extension of the work in ref. [12], and follows closely the analytical solutions presented by Shapiro and Motakef [19]. The basic assumptions are discussed in refs. [12, 18].

The physical situation for the slab is depicted in Fig. 2. In general, the water vapour entering the slab at the warm exposed face moves towards the cold plate. When the local water vapour concentration exceeds the saturation concentration, condensation takes place. The vapour that reaches the impermeable cold plate condenses at this surface. As time proceeds, more liquid is collected at the cold plate and the liquid pressure generated at this surface forces the liquid towards the warm, drier face. This movement is also helped by the surface tension forces. The liquid front, eventually reaches the exposed surface. No liquid was observed to drip at this surface, presumably due to the large surface tension forces that need to be overcome at the exposed surface.

The accumulation of liquid water in the slab has two important effects. These are: (i) decrease in the local vapour diffusion coefficient and (ii) increase in the local 'solid' thermal conductivity of the slab. These factors will influence both the heat flux at the cold plate and the rate of condensation in the slab.

It is clear from the experimental heat flux variations and temperature profiles shown in Figs. 3 and 4, respectively, that energy transfer and vapour diffusion may be assumed quasi-steady in relation to the liquid transport process. Similar assumptions were made by Shapiro and Motakef [19] on the basis of time-scale analysis.

For the wet region, the temperature distribution is obtained from the energy equation [12]:

$$\frac{\mathrm{d}}{\mathrm{d}z}\left\{(k(\theta)+\rho_a D_0(\theta)h_{fg}g'(T))\frac{\mathrm{d}T}{\mathrm{d}z}\right\}=0 \qquad (1)$$

where

$$g(T)=\bar{C}\exp\left[a\left(\frac{1}{T_0}-\frac{1}{T}\right)\right] \qquad (2)$$

and $g(T)$ is the Clausius–Clapeyron relation for the saturation vapour concentration at the local temperature, T. For the temperature range of about 0–58°C, the following numerical values at the mean tem-

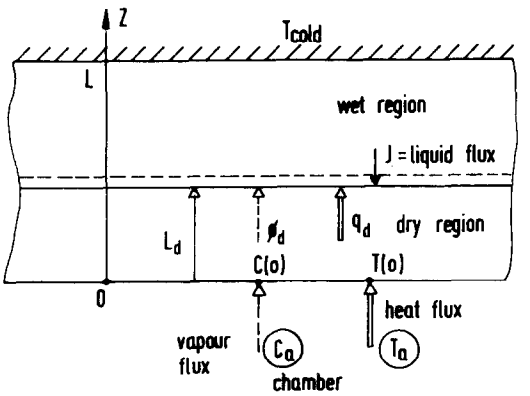

FIG. 2. Physical situation in the slab.

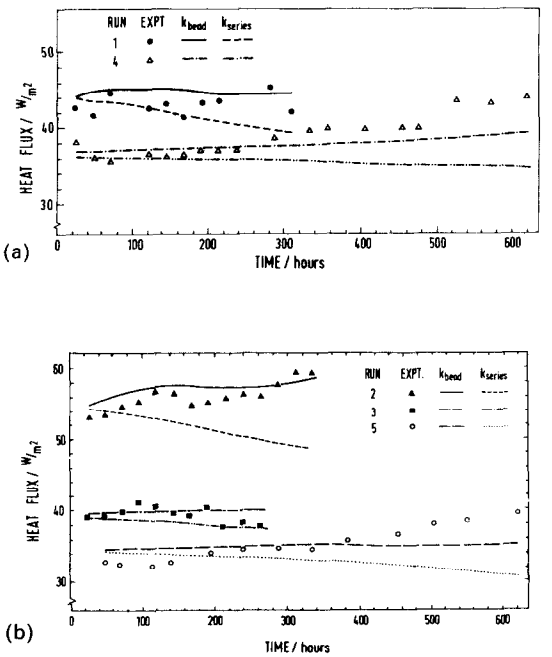

FIG. 3. (a) Variation of heat flux at cold surface with time. (b) Variation of heat flux at cold surface with time.

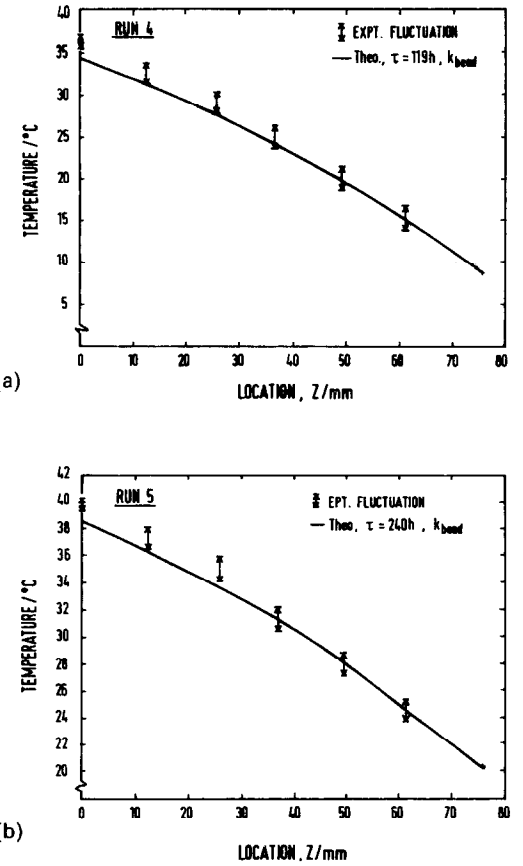

FIG. 4. (a) Temperature distribution in slab: run 4. (b) Temperature distribution in slab: run 5.

perature are used:

$$T_0 = 302\ \text{K}, \quad a = 5271.2 \quad \text{and} \quad \bar{C} = 0.0232.$$

In the dry region, the vapour mass conservation equation and the energy equation are uncoupled and for constant values of D_0 and k, these equations have simple solutions [12].

Boundary conditions

The following mass and energy balance may be written at the dry–wet interface

$$-D_0\rho_a\left.\frac{dC}{dz}\right|_{L_d} = \phi_d + J + \theta_d\frac{dL_d}{dt} \tag{3}$$

$$-k\left.\frac{dT}{dz}\right|_{L_d} = q_d - h_{fg}J - h_{fg}\theta_d\frac{dL_d}{dt}. \tag{4}$$

Since saturated conditions exist at the dry–wet interface, equations (3) and (4) can be simplified to:

$$\left\{(k + h_{fg}D_0\rho_a g'(T))\frac{dT}{dz}\right\}_{L_d} = -(q_d + h_{fg}\phi_d). \tag{5}$$

When the dry–wet interface has reached the exposed surface at $z = 0$, the boundary conditions may be assumed to be

$$-D_0\rho_a\left.\frac{dC}{dz}\right|_0 = h_m(C_a - C(0)) + J \tag{6}$$

and

$$-k\left.\frac{dT}{dz}\right|_0 = h(T_a - T(0)) - h_{fg}J. \tag{7}$$

These lead to the equation

$$\left\{(k + h_{fg}\rho_0 D_a g'(T))\frac{dT}{dz}\right\}_0 = -h_{fg}h_m(C_a - C(0)) - h(T_a - T(0)). \tag{8}$$

Solution procedure

The temperature and vapour flux distribution in the wet region are obtained by solving the governing equation (1) with boundary conditions (5) or (8), depending on the location of the dry–wet interface as mentioned earlier. The heat flux, q_d, and the vapour flux, ϕ_d, in the dry region are obtained as

$$q_d = -k\left.\frac{dT}{dz}\right|_{L_d} = [T_a - T(L_d)]\Big/\left(\frac{1}{h} + \frac{L_d}{k_d}\right) \tag{9}$$

and

$$\phi_d = -\rho_a D_0\left.\frac{dC}{dz}\right|_{L_d} = [C_a - C(L_d)]\Big/\left(\frac{1}{h_m} + \frac{L_d}{\rho_a D_0}\right). \tag{10}$$

At the wet–dry interface,

$$\left.\frac{dC}{dz}\right|_{L_d} = g'(T)\left.\frac{dT}{dz}\right|_{L_d}. \tag{11}$$

The solution of equation (1) in the wet region requires a knowledge of the dependence of the diffusion coefficient, $D_0(\theta)$, and the 'solid' thermal conductivity, $k(\theta)$, on the local liquid concentration θ.

Simple models available in the literature [26, 27] are used to compute these properties. The vapour diffusion coefficient, $D_0(\theta)$, is given by

$$D_0(\theta) = \frac{D_a}{\tau}\varepsilon_v(\theta) \tag{12}$$

where the void fraction ε_v is dependent on the liquid content θ. This may be written as

$$\varepsilon_v(\theta) = 1 - \varepsilon_f - \frac{\theta}{\rho_\omega} \tag{13}$$

where ε_f is the volume fraction of the fibres and ρ_ω the density of water. The effect of the liquid on the tortuosity factor τ is neglected. The diffusion coefficient for the water vapour–air mixture is assumed to be (26):

$$D_a = 1.97 \times 10^{-5}\left(\frac{T}{255.2}\right)^{1.685} \tag{14}$$

where T is the local temperature.

The effect of liquid water on the 'solid' thermal conductivity of fibrous insulants is discussed by Batty *et al.* [27]. Two possible models for k are considered in the present study.

(a) *Series arrangement.* In this model water is distributed in layers perpendicular to the direction of heat flow. The water would then have the maximum effect in inhibiting the heat flow. For the series arrangement it is easy to show that [27]

$$k(\theta) = \frac{k_d k_\omega}{k_\omega - X(\theta)} \tag{15}$$

where

$$X(\theta) = \frac{(k_\omega - k_d)\theta}{\rho_\omega(1-\varepsilon_f)}. \tag{16}$$

(b) *Bead arrangement.* In this model water is distributed uniformly as small beads throughout the insulant. Batty *et al.* [27] give the following formula for the thermal conductivity for this arrangement:

$$k(\theta) = k_d \frac{(1+2VY)}{(1-VY)} \tag{17}$$

where

$$Y = \frac{(k_\omega - k_d)}{(k_\omega + 2k_d)} \tag{18}$$

and

$$V = \frac{\theta}{\rho_\omega}. \tag{19}$$

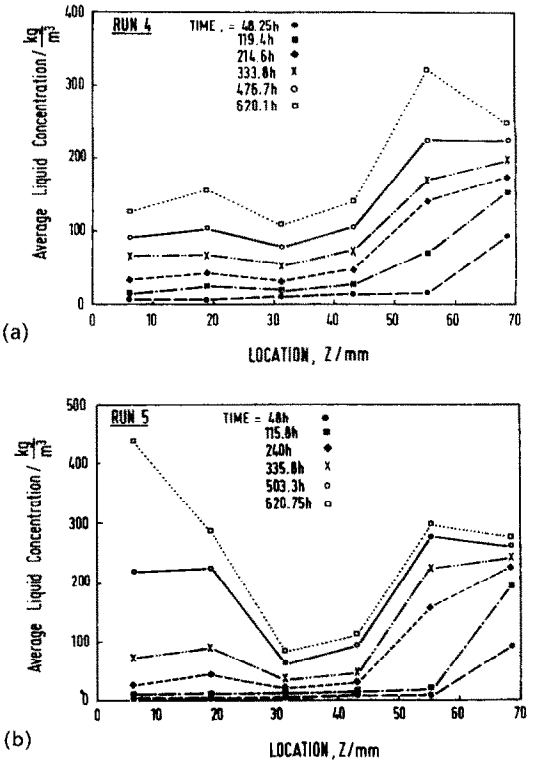

FIG. 5. (a) Liquid distribution in slab at different times: run 4. (b) Liquid distribution in slab at different times: run 5.

The actual distribution of liquid in the insulation is not completely known. However, the above models will give an indication of the sensitivity of the predicted quantities to the variations in these important physical properties.

The application of the present model requires a knowledge of the heat and mass transfer coefficients between the chamber air and the exposed insulation specimen. These were estimated experimentally. The chamber was maintained at the desired temperature with the water surface covered. The measured heat flux and the linear temperature distribution in the slab were used to estimate the heat transfer coefficient by a simple heat balance. This varied between 4 and 7 W m^{-2} K^{-1}. The mass transfer analogy [26] was applied to obtain the mass transfer coefficient.

In the present study an attempt was made to fit the diffusion coefficient $D_L(\theta)$ for liquid diffusion by matching the liquid distributions with those shown in Figs. 5(a) and (b). This one-dimensional procedure did not yield satisfactory results. A two-dimensional model of the form described by Vafai and Tien [22] may have to be used for this purpose. In view of these difficulties, it was decided to use the experimentally determined liquid distribution histories in the solution of equation (1) for the temperature and vapour flux variation. Further work, under isothermal conditions, needs to be done to determine the diffusion coefficients for liquid transport perpendicular to the fibers in fiberglass slabs. Some experimental work in this direction was reported recently by Prazak *et al.* [28], and Cid and Crausse [29].

The solution of equations (1), (9) and (10) is obtained by the following iterative method. An initial trial value is assumed for the dry–wet interface temperature $T(L_d)$. The corresponding value of the concentration, $C(L_d)$, is obtained from equation (2). These values are substituted in equations (9) and (10) to obtain the dry region length L_d. For the wet region, equation (1) is solved using the predictor–corrector method starting from the dry–wet interface. This gives the temperature of the cold surface, which is compared with the actual cold surface temperature. $T(L_d)$ is adjusted until the predicted cold surface temperature matches the actual temperature.

For the wet region, the nodal values of the thermal conductivity, $k(\theta)$, and diffusion coefficient, $D_0(\theta)$, are obtained from the various models described above.

At the start of each new time interval, the experimentally determined liquid distribution is compared with the calculated dry–wet interface position to determine whether water has diffused to the 'dry' region. If this has happened, then the wet–dry interface position is shifted to the location given by the experimental data, and the calculation is repeated. There is some uncertainty in this procedure because the water

front does not seem to move in the well defined manner that is assumed in most analyical formulations [18, 19]. In the present study, a moisture content in excess of 50 kg m^{-3} is assumed to be caused by liquid movement, while values below this are assumed to be due to local condensation. However, it should be noted that the predicted quantities are not very sensitive to the exact location of the dry–wet interface under the present conditions.

When the dry–wet interface has moved to the exposed surface at $z = 0$, equation (1) is solved in the same manner as for the wet region but using the boundary condition given by equation (8).

Three important measured quantities can be compared with those predicted by the foregoing procedure. These are: (i) the temperature distribution histories, (ii) the heat flux at the cold surface given by the integration of equation (1), and (iii) the total moisture gain by the slab.

The heat flux at the cold surface is given by

$$q_L = \left[k + \rho_a D_0 h_{fg} g'(T) \frac{dT}{dz}\right]_{z=L}. \quad (20)$$

The total moisture gain per unit volume of the slab is obtained by applying the mass conservation equation to the entire slab in the form

$$\Delta W = \frac{1}{L}\int_0^{\Delta\tau} h_m[C_a - C(0)]\,dt. \quad (21)$$

Equation (21) is integrated numerically using the quasi-steady values of the concentration $C(0)$ at the exposed surface. This is obtained from the solution of the vapour diffusion equation.

In the next section of the paper, the experimental results are presented and their comparison with the foregoing predictions is discussed.

RESULTS AND DISCUSSION

Condensation and liquid transport

The measurement of the rate of condensation and liquid transport within the insulation slab involves several sources of uncertainty. The mass of each layer was measured with an accuracy of 0.1 g. The total moisture gain during the measurement time of 10 min is estimated to be about 0.8 g. Both these quantities are much smaller than the total moisture gain between two consecutive measurements which is about 120 g.

The resistance thermometers used to monitor the temperature of the chamber were calibrated to an accuracy of 0.1°C. The temperature of the chamber remained stable within about ±0.2°C, over the entire testing time of about 300–600 h. The fluctuation of the relative humidity was about ±3%.

Seven test runs were performed with different slabs of fiberglass, covering a range of experimental conditions. The details of these test runs are summarized in Table 1.

The distribution of the average liquid concentration at different locations in the slab was obtained by measuring the increase in mass of the different layers. The variation of the average liquid concentration with time is shown in Figs. 6(a)–(e) for the different runs. The spatial distribution of the liquid concentration at different times is shown in Figs. 5(a) and (b) for two runs. These curves display similar trends of variation. Initially, vapour condensation occurs mainly at the cold surface. The liquid produced is deposited in the insulation layer adjacent to the cold plate because of the presence of the vapour barrier on the insulation. The rate of moisture gain at this stage is nearly constant. Because of the pressure generated at the cold plate due to condensation, the liquid is forced towards the next layer. When the liquid paths enter the second layer, there is a marked increase in the liquid concentration in that layer and a corresponding reduction in the rate of increase of liquid mass in the first layer. For run 1 (Fig. 6(a)), this transition occurs at about 60 h. As time proceeds, the liquid penetrates into the adjoining layers with the resultant increase in their liquid content and a corresponding levelling off of the liquid mass in the upstream layers. In addition to this mechanism, there is also a change in the liquid concentration due to local condensation (or evaporation).

A careful scrutiny of the above curves for the different runs shows that, although the aforementioned behaviour is generally true, in some instances the liquid path seems to penetrate two layers

Table 1. Details of experimental conditions

Test run No.	Duration of test (h)	Slab thickness (mm)	Mean density (kg m^{-3})	Temp. of cold plate (°C)	Dry bulb temp. chamber (°C)	Mean relative humidity
1	310	62.0	54	20.8	40.5	97%
2	340	68.7	54	13.0	40.5	96.5%
3	264	70.0	34	7.5	35.5	96%
4	620	76.1	56	8.5	36.4	96%
5	620	76.1	56	20.4	40.0	95.5%
6	190	75.0	54	16.0	43.0	96%
7	300	77.6	55	20.8	40.1	97%

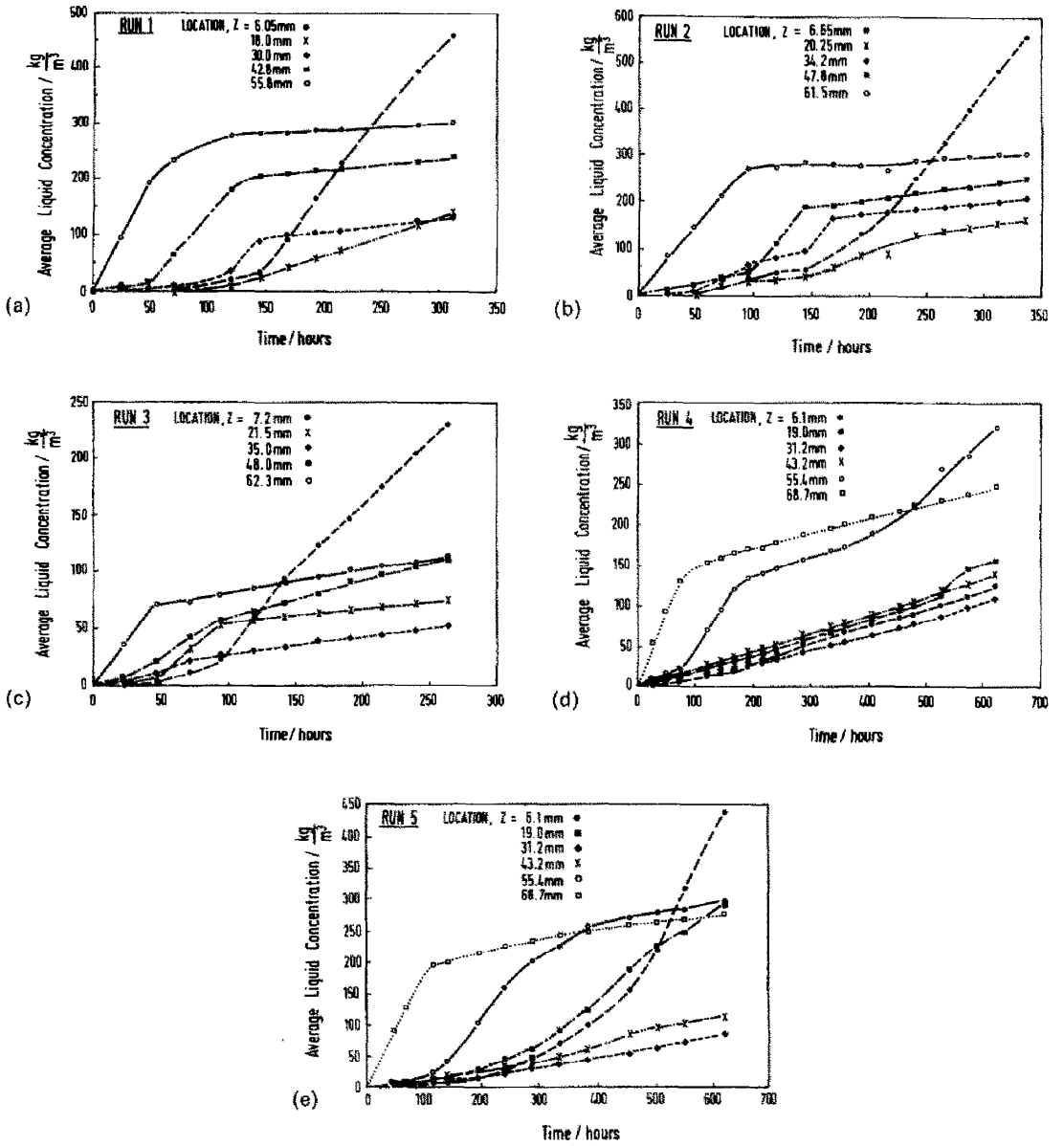

FIG. 6. (a) Variation of average liquid concentration with time: run 1. (b) Variation of average liquid concentration with time: run 2. (c) Variation of average liquid concentration with time: run 3. (d) Variation of average liquid concentration with time: run 4. (e) Variation of average liquid concentration with time: run 5.

during the test period. Such a situation is evident in Fig. 6(c) for run 3. In the present tests, the heat and vapour flow was perpendicular to the orientation of the fibres, which is usually the case with fibreglass insulations in practice. The capillary rise of water perpendicular to the fibres in fibreglass is very small [15]. Motakef and El-Masri [14] proposed that the liquid transfer perpendicular to the fibres is due to a combination of liquid movement along the fibers by capillary pressure and a sudden penetration of the liquid into the next fibre layer. This is believed to be due to the presence of fibres that 'cross' from one layer to the next. In the present situation, there is also the liquid pressure at the plate in addition to the mechanism proposed in ref. [14].

The sharp turning points of the curves in Figs. 6(a)–(d), can be taken as an indication of the times for the liquid 'front' to cross an interface. By fitting a curve to this data, the position of the liquid 'front', z_0, was found to be proportional to, $t^{1.77}$, for the present experiments. This is different from the variation, $z_0 \propto t^{0.5}$, that is expected from a balance between the surface tension forces and viscous forces [14].

In order to obtain further insight into the liquid transport process, a water soluble dye was placed at the vapour barrier for run 6. The distribution of the

dye in the different layers after 190 h is shown in Fig. 7. It was found that some areas of the insulation layers remained almost completely dry while other areas were saturated with water. Moreover, after some 'wet paths' have been established, these paths seem to be used preferentially for subsequent liquid transport. Since there is a tendency for liquid movement along the fibres, the edges of the slab also play a part in the liquid transfer. Although a plastic liquid barrier was applied to the edges in the present test, liquid could be transferred between adjacent layers across the edges. The dye distribution in Fig. 7 appears to indicate this. The effect of gravity on liquid transfer was investigated by leaving the moisture laden insulation slab in the test cavity for several days under isothermal conditions. Subsequent weighing showed that liquid transfer between layers, if any, to be negligibly small.

An interesting observation is the rapid rise in the liquid concentration of the layer with the exposed surface. This usually occurs after the liquid paths have penetrated this layer. One reason for this behaviour, is the tendency of this layer to accumulate water due to the surface tension forces between the water and the last layers of fibres at the exposed surface. No dripping of water was observed at this surface.

The computed variation of the net condensation rate at different locations (layers) in the insulation slab is shown in Figs. 8(a) and (b). It is seen that, with time, the condensation rate in the exposed layer increases. This is due to the temperature variation caused by the increased thermal conductivity of the slab which is a result of the increased liquid content. The complex changes in the condensation rate occurs only when the liquid concentration is high.

The computed condensation (or evaporation) rates, and the measured mean liquid concentrations, θ, were substituted in the numerical form of the liquid diffusion equation [19], to obtain the variation of the mean liquid fluxes at the interfaces. These fluxes in turn were used to deduce the values of the mean liquid diffusion coefficient D_L. The computed D_L showed large fluctuations for the early part of the run. However, at longer times, the value of D_L varied from about 10^{-9} to 8×10^{-9} m^2 s^{-1}. These value are of the same order as those reported by Cid and Crausse [29].

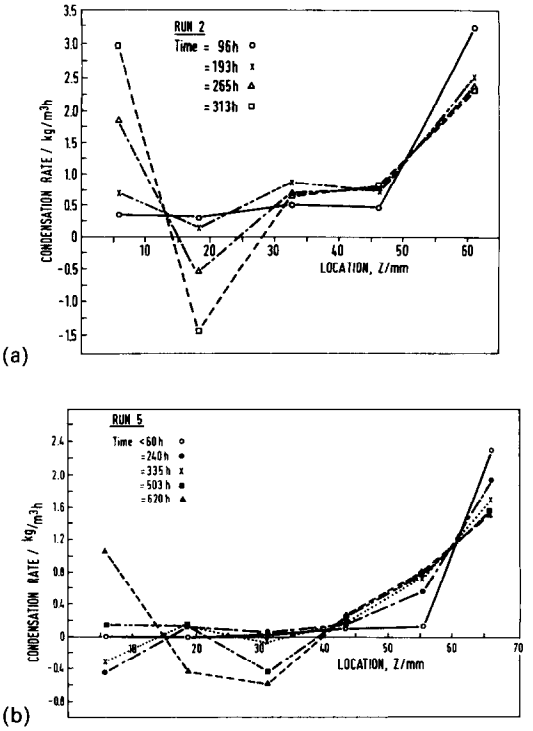

FIG. 8. (a) Computed distribution of condensation rate in slab at different times: run 2. (b) Computed distribution of condensation rate in slab at different times: run 5.

The variation of the total moisture gain by the slab is shown in Figs. 9(a), (b) and (c). Also indicated are the corresponding computed values for the two models assumed for the thermal conductivity. Both models show good agreement with measurements at the early part of the runs. However, at longer times, the measured rate of moisture gain is smaller than that predicted by the models. This may be due to the inadequacy of the simple model used to account for the decrease in the vapour diffusion coefficient with liquid concentration.

Varying the heat transfer coefficient at the exposed surface from 4 to 7 W m^{-2} K^{-1}, and substituting the corresponding values of the mass transfer coefficient, changed the computed total moisture gain by about 6%.

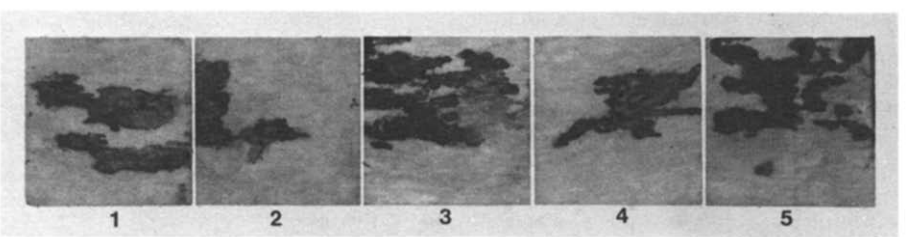

FIG. 7. Dye distribution at different locations at time = 190 h: run 6. (1) $z = 8$ mm, $\theta = 400$ kg m^{-3}; (2) $z = 23.5$ mm, $\theta = 151$ kg m^{-3}; (3) $z = 38$ mm, $\theta = 229$ kg m^{-3}; (4) $z = 52.5$ mm, $\theta = 155$ kg m^{-3}; (5) $z = 67.5$ mm, $\theta = 233$ kg m^{-3}.

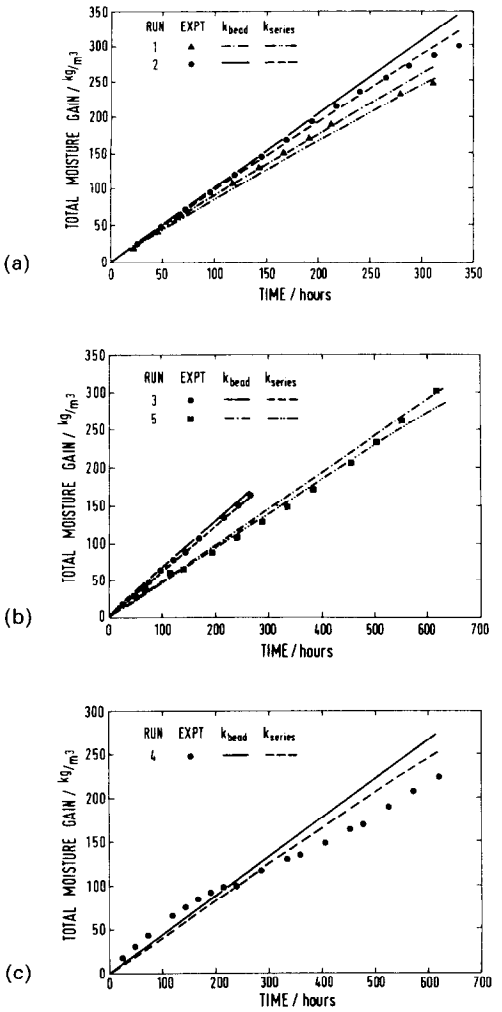

FIG. 9. (a) Variation of total moisture gain by slab with time. (b) Variation of total moisture gain by slab with time. (c) Variation of total moisture gain by slab with time.

Variation of heat flux

The main uncertainty in the heat flux measurement is the calibration of the heat flux meter. The calibration curve supplied by the manufacturer was checked by measuring the thermal conductivity of a standard insulation specimen [25] over the temperature range of interest. The maximum deviation was about 6%. The heat flux meter calibration curve was adjusted to reproduce the thermal conductivity of the standard specimen, which has an estimated uncertainty of about 2%.

The variation of the heat flux for different test runs is shown in Figs. 3(a) and (b). Also indicated are the computed heat flux using the two thermal conductivity models. It appears that the 'bead model' gives better trend-wise agreement with the measured heat flux for all the runs. The heat flux reaching the cold plate has two components. The first is due to conduction which depends on the 'solid' thermal conductivity of the moisture laden insulation. The second component is due to the condensation of the vapour within the slab. The latter decreases with time due to the reduction in the total moisture gain (Figs. 9(a)–(c)) with time. However, the total heat flux shows an increasing trend with time, which suggests that the thermal conductivity has to increase adequately to bring this about.

At a water volume fraction of 0.25 in an insulation of dry thermal conductivity 0.035 W m^{-1} K^{-1}, the 'bead' model gives a thermal conductivity of 0.063 W m^{-1} K^{-1}, while the corresponding value for the 'series' model is 0.046 W m^{-1} K^{-1}.

Varying the heat transfer coefficient at the exposed surface from 4 to 7 W m^{-2} K^{-1} changed the computed heat flux by about 2.5%.

It is important to note that the insulation slab undergoes dimensional changes due to the absorption of water. For run 5 this was about 1.5 mm when the total moisture gain is about 150 kg m^{-3} and about 3 mm when the moisture gain is 215 kg m^{-3}. These dimensional changes have not been taken into account in the quasi-steady model.

Temperature distribution

The uncertainty in the temperature measurement was ± 0.1°C due to the accuracy of calibration of the thermocouples. There was also an uncertainty of about 1–2 mm in the position of the thermocouples located at the interfaces. This is due to the soft nature of the fibreglass layers.

Typical temperature distributions are shown in Figs. 4(a) and (b). The temperature fluctuation at the different locations during the entire run was less than about 3°C. The fluctuation in the computed temperature was only about 0.5°C. There is trend-wise agreement between the measured and computed temperature distributions. The dimensional changes of the slab and the position uncertainty of the thermocouples may be partly responsible for the observed fluctuations. The measured variation of the temperature at different locations with time is shown in Fig. 10.

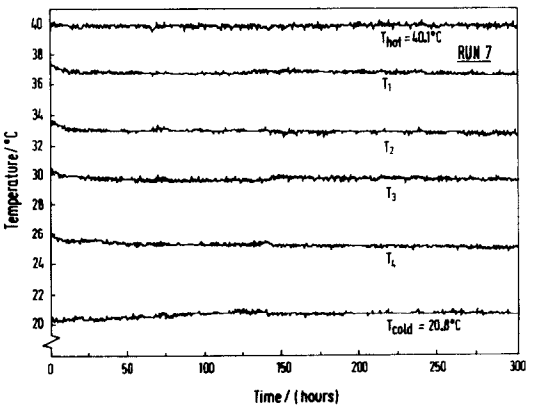

FIG. 10. Variation of temperature at different points with time: run 7.

Qualitative comparison of the trends can be made between the present experimental data and the two-dimensional simulations of Vafai and Tien [22]. Although the boundary conditions are not identical for the two situations, it is seen that in both cases the spatial temperature gradient at the centre of the slab cross-section increases gradually from the region of low condensation to the region of high condensation of vapour. The plots in ref. [22] show significant two-dimensional effects near the mid-section of the slab. This effect was experimentally investigated by placing thermocouples at the middle and the quarter points of the section. These did not reveal systematic two-dimensional effects and the differences in temperature at the different points were within the experimental fluctuations shown in Fig. 10. This is probably because the slab was horizontal in the present experiments while the computations in ref. [22] are for a vertical slab. The liquid distribution computed in ref. [22], shows significant two-dimensional variations. This is confirmed by the dye distribution shown in Fig. 7. The liquid distributions measured in the present experiments are averaged over layers and are therefore, one-dimensional quantities. It is clear from these comparisons that a complete interpretation of the experimental results, in particular the liquid distribution, will require a two-dimensional numerical simulation of the transport processes. Such an effort is currently being undertaken.

CONCLUSION

An experimental set-up was developed to simulate the moisture absorption by fibrous insulations. The liquid distribution, total moisture gain, heat flux, and the temperature distributions were measured. A quasi-steady, semi-empirical model was used to interpret some of the experimental observations. The liquid transport process did not follow a one-dimensional diffusion law.

The rate of total moisture gain remained nearly constant initially and gradually decreased due to liquid accumulation in the slab. The heat flux showed a very gradual increase with time. The measured temperature distribution showed a maximum fluctuation of about $\pm 3^{\circ}C$.

The predictions of the quasi-steady analysis using simple models for the effect of the liquid on the vapour diffusion coefficient and the thermal conductivity showed reasonable agreement with some of the measured quantities. However, a two-dimensional numerical model will be needed to simulate the liquid transport processes in the fibrous slab.

Acknowledgements—The authors acknowledge with gratitude a grant awarded under the ASEAN-Australian Economic Cooperation Programme in support of the work on thermal insulation. The contribution of K. H. Yeo to the experimental work is thankfully acknowledged.

REFERENCES

1. W. A. Lotz, Moisture problems in buildings in hot humid climates, *ASHRAE J.* **31**(4), 26–27 (April 1989).
2. H. B. Jespersen, Thermal conductivity of moist materials and its measurements, *J. Inst. Heat Vent. Engrs* **1**, 216–222 (1953).
3. F. A. Joy, Symposium on thermal conductivity measurements and applications of thermal insulations, *ASTM STP* **217**, 65–80 (1957).
4. W. Woodside, Probe for thermal conductivity measurements of dry and moist materials, *Heat Pipe. Air Cond.* **30**, 163–170 (1958).
5. L. C. Langlais, M. Hydrien and S. Klarsfeld, Influence of moisture on heat transfer through fibrous insulating materials. In *Thermal Insulation, Materials and Systems for Energy Conservation in the '80s* (Edited by F. A. Govan, D. M. Greason and J. D. McAllister), *ASTM STP* **789**, 563–581 (1983).
6. W. C. Thomas, G. P. Bal and R. J. Onega, Heat and mass transfer in glass fiber roof insulating materials, *ASTM STP* **789**, 582–601 (1983).
7. C. Langlais and S. Klarsfeld, Heat and mass transfer in fibrous insulation, *J. Therm. Insulat.* **8**, 49–80 (July 1984).
8. M. K. Kumaran, Moisture transport through glass-fibre insulation in the presence of a thermal gradient, *J. Therm. Insulat.* **10**, 243–255 (April 1987).
9. C. P. Hedlin, Heat transfer in a wet porous thermal insulation in a flat roof, *J. Therm. Insulat.* **11**, 165–188 (January 1988).
10. D. K. Modi and S. M. Benner, Moisture gain of spray applied insulations and its effect on effective thermal conductivity—Part I, *J. Therm. Insulat.* **8**, 259–277 (April 1985).
11. S. M. Benner and D. K. Modi, Moisture gain of spray-applied insulations and its effect on effective thermal conductivity—Part II, *J. Therm. Insulat.* **9**, 211–223 (January 1986).
12. N. E. Wijeysundera, M. N. A. Hawlader and Y. T. Tan, Water vapour diffusion and condensation in fibrous insulations, *Int. J. Heat Mass Transfer* **23**, 1865–1878 (1989).
13. N. E. Wijeysundera, M. N. A. Hawlader and S. C. Lian, An experimental study of condensation in fiberglass insulations, Paper FE89-32, ASHRAE Far East Conf. on Air Conditioning in Hot Climates, Kuala Lumpur, Malaysia (25–28 October 1989).
14. S. Motakef and M. A. El-Masri, Liquid diffusion in fibrous insulation, *J. Heat Transfer* **107**, 229–306 (May 1985).
15. J. Timusk and L. M. Tenende, Mechanism of drainage and capillary rise in glass fibre insulation, *J. Therm. Insulat.* **11**, 231–241 (April 1988).
16. P. Crausse, G. Bacon and C. Langlais, Experimental and theoretical study of simultaneous heat and moisture transfer in a fibrous insulation, *J. Therm. Insulat.* **9**, 46–67 (July 1985).
17. Y. Ogniewiez and C. L. Tien, Analysis of condensation in porous insulation, *Int. J. Heat Mass Transfer* **24**, 421–429 (1981).
18. S. Motakef and M. A. El-Masri, Simultaneous and heat and mass transfer with phase change in a porous slab, *Int. J. Heat Mass Transfer* **29**, 1503–1512 (1986).
19. A. P. Shapiro and S. Motakef, Unsteady heat and mass transfer with phase change in porous slab: analytical solutions and experimental results, *Int. J. Heat Mass Transfer* **33**, 163–173 (1990).
20. K. Vafai and S. Sarkar, Condensation effects in a fibrous insulation slab, *J. Heat Transfer* **108**, 667–675 (August 1986).
21. K. Vafai and S. Whitaker, Simultaneous heat and mass transfer accompanied by phase change in porous insu-

lation, *J. Heat Transfer* **108,** 132–140 (February 1986).
22. K. Vafai and H. C. Tien, A numerical investigation of phase change effects in porous materials, *Int. J. Heat Mass Transfer* **32,** 1261–1277 (1989).
23. H. C. Tien and K. Vafai, A synthesis of infiltration effects on an insulation matrix, *Int. J. Heat Mass Transfer* **33,** 1263–1280 (1990).
24. ASTM-C518, *Steady-state Thermal Transmission Properties by Heat Flow Meter Method.* ASTM, Philadelphia, U.S.A. (1976).
25. B. G. Rennex, R. R. Jones and D. G. Ober, Development of calibrated transfer specimens of thick low-density insulations, *Proc. Int. Thermal Conductivity Conf.*, Gaithersburg, U.S.A., pp. 419–426 (15–18 June 1981).
26. D. K. Edwards, V. E. Denny and A. F. Mills, *Transfer Process.* McGraw-Hill, New York (1976).
27. W. J. Batty, P. W. O'Callaghan and S. D. Probert, Apparent thermal conductivity of glass-fibre insulant: effect of compression and moisture content, *Appl. Energy* **9,** 55–76 (1981).
28. J. Prazak, J. Tywonik, F. Peterka and T. Slonc, Description of transport of liquid in porous media, *Int. J. Heat Mass Transfer* **33,** 1105–1120 (1990).
29. J. Cid and P. Crausse, Influence of the structural characteristics of fibrous heat insulators upon their properties of moisture transfer, *J. Therm. Insulat.* **14,** 123–134 (October 1990).

EFFETS DE LA CONDENSATION ET DU TRANSPORT DE LIQUIDE SUR LA PERFORMANCE THERMIQUE DES ISOLANTS FIBREUX

Résumé—Le gain d'humidité par un isolant fibreux en plaque dans une ambiance humide est simulé dans des conditions de laboratoire. La distribution de liquide, le gain total d'humidité, le flux thermique et la distribution de température sont mesurés dans un domaine de conditions expérimentales. Les temps d'essais vont de 300 à 600 heures. Les mécanismes physiques dans le transport de liquide sont identifiés. Initialement le gain total d'humidité croît presque linéairement avec le temps, puis décroît graduellement. Le flux thermique montre un accroissement très graduel avec le temps. Le modèle semi-empirique utilisé donne des prédictions raisonnables sur les grandeurs mesurées.

EINFLUSS VON KONDENSATION UND FLÜSSIGKEITSTRANSPORT AUF DAS THERMISCHE VERHALTEN FASERIGER ISOLATIONSMATERIALIEN

Zusammenfassung—Unter Laborbedingungen wird die Feuchtigkeitsaufnahme einer faserigen Isolationsmatte aus der feuchten Umgebung simuliert. Die Flüssigkeitsverteilung, die gesamte Feuchteaufnahme, sowie die Verteilungen von Wärmestromdichte und Temperatur werden unter unterschiedlichen Versuchsbedingungen gemessen. Die Versuchsdauer liegt im Bereich zwischen 300 und 600 Stunden. Die physikalischen Vorgänge, die mit dem Flüssigkeitstransport verbunden sind, werden identifiziert. Anfänglich nimmt die insgesamt aufgenommene Feuchte fast linear mit der Zeit zu, um dann langsam abtufallen. Die Wärmestromdichte steigt mit fortschreitender Zeit sehr langsam an. Das verwendete halbempirische Modell ermöglicht die brauchbare Vorhersage einiger der gemessenen Größen.

ВЛИЯНИЕ КОНДЕНСАЦИИ И ПЕРЕМЕЩЕНИЯ ВЛАГИ НА ТЕПЛОВЫЕ ХАРАКТЕРИСТИКИ ВОЛОКНИСТЫХ ИЗОЛЯЦИЙ

Аннотация—В лабораторных условиях моделируется поглощения влаги из окружающей среды волокнистой изоляционной пластиной. Определяются распределение жидкости, суммарное поглощение влаги, а также тепловой поток и распределение температур для широкого диапазона условий эксперимента. Продолжительность экспериментов изменялась от 300 до 600 часов. Выявляются физические процессы, происходящие при перемещении влаги. Вначале суммарное поглощение влаги возрастает почти линейно со временем, а затем постепенно снижается. Тепловой поток увеличивается со временем весьма медленно. Использование полуэмпирической модели позволяет с удовлетворительной точностью прогнозировать некоторые экспериментальные данные.